IEEE Access
Multidisciplinary | Rapid Review | Open Access Journal

Received November 5, 2018, accepted November 19, 2018, date of publication November 30, 2018,
date of current version December 31, 2018.

Digital Object Identifier 10.1109/ACCESS.2018.2884218

Dynamic Switching of Two Degree-of-Freedom Control for Belt-Driven Servomechanism

CHUN-LIN CHEN, Student Member, IEEE, AND MI-CHING TSAI, Senior Member, IEEE
Department of Mechanical Engineering, National Cheng Kung University, Tainan 70101, Taiwan

Corresponding author: Mi-Ching Tsai (mctsai@mail.ncku.edu.tw)

This work was supported by the Ministry of Science and Technology (MOST), Taiwan, under Grant MOST 106-2221-E-006-251-MY3 and Grant MOST 106-2218-E-006-023.

ABSTRACT This paper proposes a new two degree-of-freedom control structure such that the robustness control of a belt-driven servomechanism is adequately addressed. In conventional design approaches, a trade-off between robust stability and robust tracking performance is unavoidable because the control engineer must take different frequency regions into consideration. In this paper, a frequency-dependent switching control structure is proposed, where the feedback connection to the external-loop controller is dynamically switched between the outputs of the controlled plant and its nominal model. The disturbance attenuation at lower frequencies by the double-loop control, as well as the robust stability at higher frequencies through the reference feedforward control, can be achieved at one fixed two degree-of-freedom control structure. The feasibility of the proposed approach is verified by theoretical analysis and experimental results.

INDEX TERMS Servomechanism, robustness, H-infinity control, control engineering.

I. INTRODUCTION

High performance servomechanisms have become of great importance in control engineering. In order to develop an advanced control strategy, a two-mass system with a belt-driven transmission is usually investigated [1]. The degree of freedom (DOF) of a control system is defined as the number of closed-loop transfer functions that can be designed independently [2]. For a single DOF control scheme, it is difficult to simultaneously meet the various performance requirements, such as the tracking performance, disturbance attenuation, and robust control requirements. Therefore, the two degree-of-freedom (TDOF) control approach has been employed to overcome this deficiency [3]–[5].

In various TDOF approaches, the PID based TDOF control structure is adopted for industrial application due to its simplicity [6]. The PI/PID mixed control scheme [7], robust optimal tuning [8], and internal model based approaches [9] show different design flexibilities and tuning methods. Moreover, the cascade double-loop structure is an alternative approach for TDOF control, which consists of an internal compensation loop for robustness and an external control loop for desired tracking performance. The disturbance observer based control system is considered as one of the most popular TDOF double-loop approaches because of its simple design procedure [10], [11]. To avoid the stability problem of inverse dynamics, the double-loop control structure was developed as an enhanced method for disturbance observer based control structure [12]–[17]. Another TDOF scheme, namely the reference feedforward control structure, was investigated for robust motion control [18]–[21]. The main difference between the double-loop and reference feedforward control structures is that the output of the controlled plant or its nominal model is adopted to the external feedback control loop. By using the controlled plant output as feedback to the external controller, the effects caused by dynamic perturbation and disturbance can be compensated by both the internal and external loops in a double-loop control structure. In contrast, the nominal model output is utilized in the reference feedforward control structure. Herein, the external control loop only generates feedforward control signals as the reference tracking response. Instead of enhancing disturbance attenuation, this structure could guarantee robust stability, which is directly designed with an internal-loop compensator.

However, it can be found in conventional TDOF control approaches that robust tracking performance and robust stability cannot easily be achieved using one fixed TDOF control scheme because of its topology constraints. The parameter tuning process for TDOF control scheme is complicated and

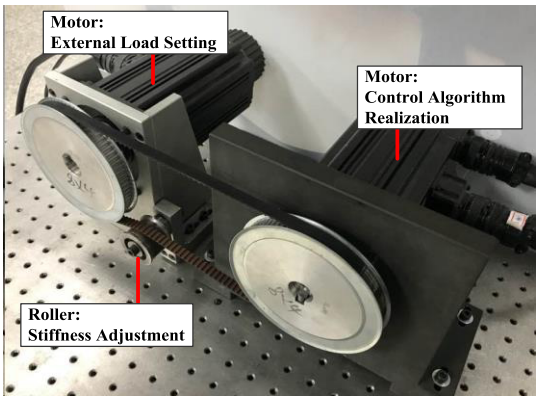

FIGURE 1. Belt-driven servomechanism.

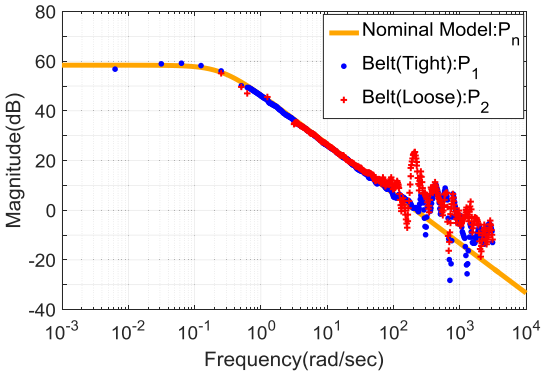

FIGURE 2. Magnitude response of belt-driven transmission.

depends on the engineer's experience. For practical applications, the dynamic perturbations, so-called modeling uncertainties, are usually of a high frequency nature, while the disturbance could occur in a low frequency range. These control performances should be designed in accordance with different operating frequencies. A control system is usually required to exhibit the satisfactory disturbance rejection for robust tracking performance within the region of low frequencies, while robust stability should be ensured at high frequencies. Therefore, to overcome the discontinuous problem resulting from the hard-switching, this study proposes a frequency-dependent switching TDOF control structure that is endowed with a dynamically switching mechanism of output feedback either from the controlled plant and/or its nominal model without changing the designed controllers. In fact, this frequency-dependent switching control structure mixes the double-loop and reference feedforward control structures by weighting output responses in accordance with the corresponding frequency. At lower frequencies, this new TDOF control scheme enhances the disturbance rejection. At higher frequencies, it keeps the robust stability and improves the dynamic tracking based on the command feedforward. Without increasing the complexity, the design dilemmas appearing in conventional TDOF control approach can be resolved. A straightforward design procedure for internal- and external-loop controllers is also provided in this study. The design example based on a belt-driven servomechanism is given to illustrate the systematic analysis and controller design procedure. Both the simulation and experimental results verify the feasibility of the proposed dynamic switching TDOF control framework.

II. SYSTEM CONFIGURATION AND SINGLE DOF CONTROL

A. BELT-DRIVEN SERVOMECHANISM

The belt-driven servomechanism in this study is depicted in Fig. 1. The experimental setup consists of a tooth-belt and two electric motors for control algorithm realization and setting external torque load. The magnitude response of the Bode plot is measured by a spectrum analyzer as shown in Fig. 2. In practice, the transmission characteristic will change gradually due to the varied belt tension. A roller is utilized to obtain different magnitude responses with a tight or loose belt, denoted by P_T and P_L, respectively. The belt-driven mechanical system also incorporates undesired flexible linkage effects, which are quite difficult to characterize and often regarded as the modeling uncertainties in control system design. Let the belt-driven mechanical system P be modeled with a given nominal model P_n and the multiplicative uncertainty such that P is formulated by

$$P = P_n\left(1 + W_u\Delta\right), \tag{1}$$

where P_n is found to characterize the measured magnitude responses for certain low-frequencies as shown in Fig. 2. Note that Δ is a norm-bounded uncertainty with $\|\Delta\|_\infty \leq 1$, where $\|\bullet\|_\infty$ denotes the H_∞ norm [22]. Moreover, W_u is the uncertainty bound transfer function, which satisfies $|W_u(j\omega)| \geq \left|\frac{P}{P_n}(j\omega) - 1\right|$.

B. DESIGN OF ROBUST STABILIZING CONTROLLER

A motion control system design should assure the specified robust stability and disturbance rejection in spite of the variation of transmission stiffness. In order to obtain the robust motion controller, a typical mixed-sensitivity design problem is considered here. Let K be the feedback controller to be designed; r and d are the input command and external disturbance, respectively, and y the controlled plant output. Moreover, e and u denote the tracking error and control input, respectively. To better understand the forthcoming discussions, the input-output transfer relations are defined by

$$y = \begin{bmatrix} T_K & S_K \end{bmatrix}\begin{bmatrix} r \\ d \end{bmatrix} = \begin{bmatrix} \dfrac{KP}{1+KP} & \dfrac{1}{1+KP} \end{bmatrix}\begin{bmatrix} r \\ d \end{bmatrix}, \tag{2}$$

where the sensitivity function S_K and the complementary sensitivity function T_K $(= 1 - S_K)$ characterize the ability of disturbance rejection and command tracking, respectively. By minimizing the cost function from d to e and u, the mixed-sensitivity problem formulation is given by

$$\left\| \begin{matrix} (1+KP_n)^{-1} \\ K\,(1+KP_n)^{-1} \end{matrix} \right\|_\infty < \gamma_o, \tag{3}$$

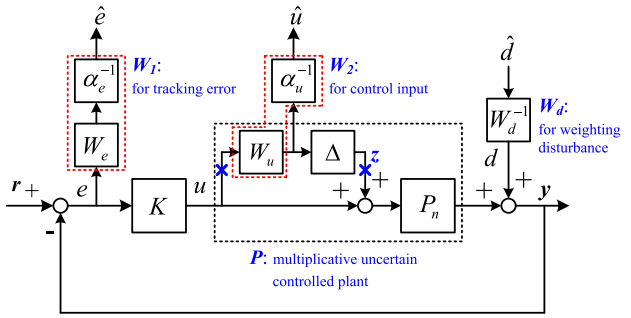

FIGURE 3. Configuration of weighted mixed sensitivity problem.

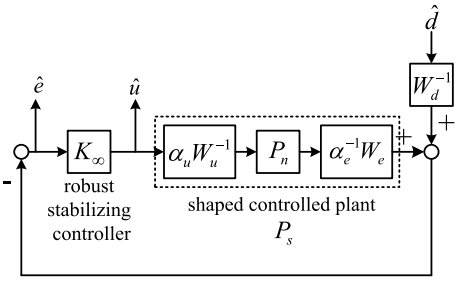

FIGURE 4. Synthesis of robust stabilizing controller by LSDP.

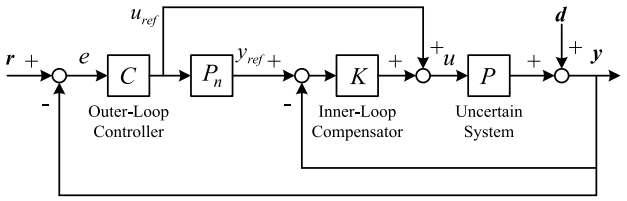

FIGURE 5. Double-loop TDOF control structure.

where γ_o is a pre-specified cost. For control system design, the performance objective in (3) should be characterized in the frequency domain. A nondimensionalization of weighted outputs is necessary to avoid the scaling problem due to different physical quantities. Therefore, the design problem configuration is shown in Fig. 3. A dimensionless cost function from $\hat{d}$ to $\hat{e}$ and $\hat{u}$ is then given by

$$\left\| \begin{bmatrix} W_1 (1 + KP_n)^{-1} \\ W_2 K (1 + KP_n)^{-1} \end{bmatrix} W_d^{-1} \right\|_\infty < \gamma_o, \tag{4}$$

where W_d, W_1, and W_2 are the predesigned weighting functions for the disturbance, tracking error, and control effort, respectively.

The loop shaping design procedure (LSDP) [23] [24] can be employed to synthesize the robust controller. By combining W_1 and W_2 into the system loop, a shaped controlled plant P_s is determined by

$$P_s(s) = \alpha_e^{-1} \alpha_u W_e P_n W_u^{-1}. \tag{5}$$

The equivalent description based on LSDP is given in Fig. 4. In this study, the practical selection of weighting functions is proposed to avoid a trial-and-error design process. Let W_1 and W_2 be firstly represented by

$$W_1 = \alpha_e^{-1} W_e \text{ and } W_2 = \alpha_u^{-1} W_u, \tag{6}$$

where each weighting function is composed of a constant weight and a frequency-dependent weight. Considering P in (1), W_u is inherently a weighting function to characterize u in the frequency domain. The weight for tracking error W_e is purposely selected to have the same characteristic poles as that of W_u. Therefore, a low order shaped plant P_s for controller design can be obtained since $W_e W_u^{-1}$ will be the coprime factorization [22]. Moreover, the constant weights α_e and α_u are directly selected from the hardware specifications of servomechanism to obtain the dimensionless weighted signals $\hat{e}$ and $\hat{u}$. As a result, a dimensionless robust design problem of (4) is given by

$$\left\| \begin{bmatrix} (1 + K_\infty P_s)^{-1} \\ K_\infty (1 + K_\infty P_s)^{-1} \end{bmatrix} W_d^{-1} \right\|_\infty < \gamma_o. \tag{7}$$

By H_∞ robust control design to synthesize K_∞ [23], the resultant robust feedback controller K is determined by

$$K(s) = \alpha_e \alpha_u^{-1} W_u K_\infty W_e^{-1}. \tag{8}$$

The stability problem with respect to modeling uncertainty is sustained by a robust stability function Ω_K, which is defined as the transfer function from z to u in Fig. 3. Note that Ω_K is equivalently the complementary sensitivity function of (2) with $P = P_n$ for the multiplicative uncertain system, i.e.,

$$\Omega_K = T_K = \frac{P_n K}{1 + P_n K}. \tag{9}$$

Based on the small gain theorem, the robust controller design procedure of (7) also implies that

$$\| \Omega_K W_u(\omega) \|_\infty \leq 1, \tag{10}$$

where Ω_K^{-1} is the allowable largest uncertainty margin of a control system. The robust stabilization solution K_∞ of (7) can be solved to enlarge system robust stability margin [23].

III. TDOF CONTROL STRUCTURE

Despite the straightforward design paradigm for K, the tracking performance requirements are usually in conflict with the system stability of a single DOF (SDOF) control system. Herein, the TDOF control structure is employed to resolve the multi-objective control design. Fig. 5 shows a TDOF scheme with a double-loop control structure, where u_{ref} and y_{ref} are the feedforward reference input and output, respectively, and C is the external loop controller. Let the controlled output y in Fig. 5 be expressed in terms of u_{ref} and d as

$$y = P_K u_{ref} + S_{CK} d, \tag{11}$$

where P_K and S_{CK} denote the internal compensation loop and the sensitivity function, respectively, and defined by

$$P_K = \frac{P(1 + KP_n)}{1 + PK}, \quad S_{CK} = \frac{1}{1 + PC + PK + PKP_nC}. \tag{12}$$

The output deviation between y and y_{ref}, which is caused by the modelling uncertainty and disturbance, can be internally compensated by K. Suppose that K has been found by solving (7) to satisfy

$$|P_K(j\omega) - P_n(j\omega)| = \left|\frac{P - P_n}{1 + PK}(j\omega)\right| \le \varepsilon\ ,\ \forall\,\omega \le \omega_R, \quad (13)$$

where ε is a small number and ω_R is the upper frequency for ensuring robustness design in the presence of uncertainty. Accordingly, P_K can behave like the nominal model P_n within a certain frequency region. The robust command tracking from r to y in Fig. 5 is given by

$$T_{CK} = \frac{PC + P_nKPC}{1 + PC + PK + P_nKPC} = \frac{P_KC}{1 + P_KC}. \quad (14)$$

Under the robustness condition of (13), (14) is rewritten as

$$\hat{T}_{CK} = \frac{P_nC}{1 + P_nC} \quad if\ \frac{y}{u_{ref}} = P_K \approx P_n,\ \forall\,\omega \le \omega_R, \quad (15)$$

where the transfer function denotes the nominal case $P_K \approx P_n$. The required tracking performance can be independently designed by the external controller C based on its nominal model P_n. In (11), the disturbance attenuation of the double loop control structure is characterized by S_{CK}. By the feedback of y, the disturbance will be further rejected by C. Assume that $P \approx P_n$ at the low frequencies $\omega \le \omega_R$, S_{CK} can be rewritten as

$$\hat{S}_{CK} = \frac{1}{(1 + P_nK)\,(1 + P_nC)} = \hat{S}_K\,S_C, \quad (16)$$

where

$$\hat{S}_K = \frac{1}{1 + P_nK}\ ,\quad S_C = \frac{1}{1 + P_nC}. \quad (17)$$

This implies that

$$\left|\hat{S}_{CK}\right| = \left|\frac{1}{(1 + P_nC)\,(1 + P_nK)}\right| \le \left|\hat{S}_K\right|\,|S_C|\,. \quad (18)$$

It can be seen that the double-loop control structure will guarantee a better disturbance attenuation than the single-loop control when $|1 + P_nC\,(j\omega)| > 1$. Considering P in (1), the robust stability function with respect to the multiplicative uncertainty is determined by

$$\Omega_{CK} = \frac{P_nC + P_nK\,(1 + P_nC)}{(1 + P_nC)\,(1 + P_nK)}. \quad (19)$$

Therefore, a well-designed C should satisfy the desired robust tracking function $\hat{T}_{CK} = \frac{P_nC}{1+P_nC}$ and robust stability $\|\Omega_{CK}W_u\|_\infty \le 1$, but also $|S_C(j\omega)| < 1$ within the frequency ω_R to enhance the disturbance attenuation. Furthermore, (19) shows that

$$\begin{aligned}|\Omega_{CK}(j\omega)| &= \left|\frac{P_nC + P_nK\,(1 + P_nC)}{(1 + P_nC)\,(1 + P_nK)}(j\omega)\right| \\ &\le \left|1 + \frac{P_nC}{(1 + P_nC)\,P_nK}(j\omega)\right|\,|\Omega_K(j\omega)|\,. \quad (20)\end{aligned}$$

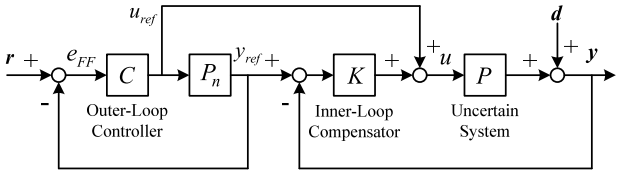

FIGURE 6. Reference feedforward TDOF control structure.

Compared with the single loop robust stabilizing control Ω_K in (9), the system stability may be degraded by the double-loop control structure if $\left|1 + \frac{P_nC}{(1+P_nC)P_nK}(j\omega)\right| > 1$. An alternative TDOF solution based on the reference feedforward control structure is represented in Fig. 6. Its main difference from the double-loop control structure is to utilize y_{ref} as the feedback of external control loop. This TDOF control approach is equivalent to the single loop control in Fig. 3, but combined with a feedforward command generator for u_{ref} and y_{ref}. The dynamic performance can be improved with the feedforward references, meanwhile the robust stability function of Ω_K given in (9) is maintained. However, the feedforward references generated by external control loop in Fig. 6 can only improve the command tracking performance. The reference feedforward control structure will lack the enhancement on disturbance attenuation since the disturbance is only rejected by K.

IV. DYNAMIC SWITCHING OF TWO CONTROL STRUCTURES

As aforementioned, the different robustness requirements may not be fully satisfied by the fixed TDOF control structure. Under the precondition of not changing the designed controllers K and C, Fig. 7(a) shows the conventional hard-switching mechanism, in that for the case of $\psi = 0$, the control system is switched to the reference feedforward control structure, and for the case of $\psi = 1$, it results in the double-loop control structure. To avoid the discontinuous switching, this study proposes a dynamic switching TDOF control framework shown in Fig. 7(b) where $\psi(s)$ is a frequency-dependent switching function. The corresponding transfer relationships from r and d to y, and the robust stability function, can be derived as

$$T_{DS} = \frac{P\,(1 + KP_n)\,C}{1 + (1 - \psi)P_nC + PK + \psi PC + PKP_nC}, \quad (21)$$

$$S_{DS} = \frac{1 + (1 - \psi)\,P_nC}{(1 + P_nC)\,(1 + PK) + \psi\,(P - P_n)\,C}, \quad (22)$$

$$\Omega_{DS} = \frac{P_nK}{1 + P_nK} + \psi\frac{P_nC}{(1 + P_nK)\,(1 + P_nC)}, \quad (23)$$

where the subscript DS denotes the dynamic switching approach. In order to endow the proposed TDOF control structure with the performances provided in Fig. 5 at low frequencies, as well as Fig. 6 at high frequencies, respectively, let the dynamic switching be selected as $\psi(s) = \frac{\omega_\psi}{s+\omega_\psi}$, where ω_ψ is a desired switching breakpoint.

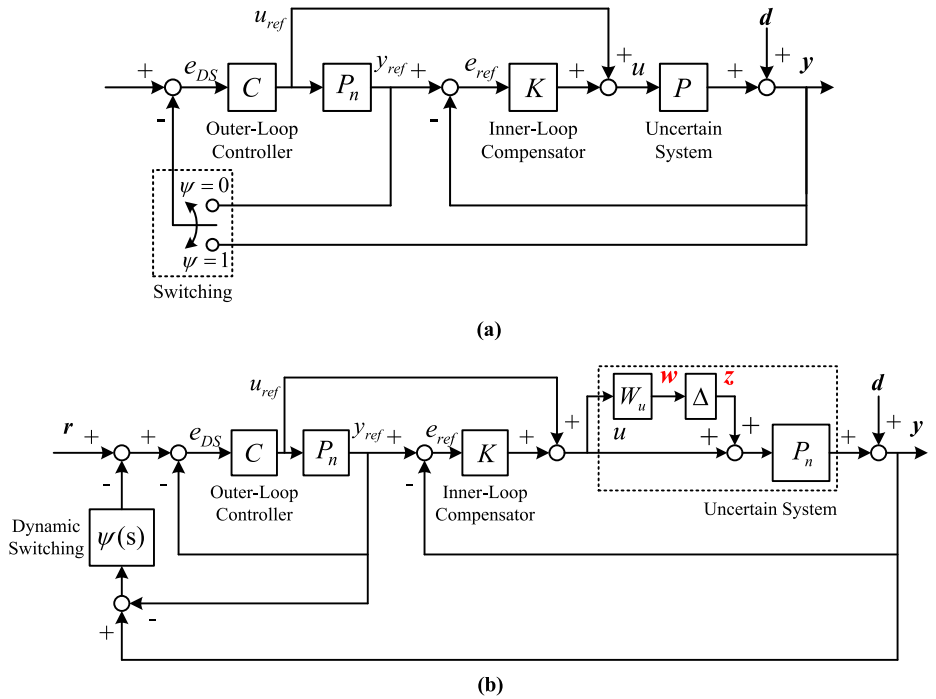

FIGURE 7. Dynamic switching TDOF control structure. (a) Hard-switching mechanism $\psi = 1$ or $\psi = 0$. (b) Frequency-dependent switching mechanism $\psi(s)$.

From Fig. 7(b), it can be observed that either the measured output feedback y or the reference output y_{ref} of the external-loop controller is used for the feedback control with the frequency-dependent switching function $\psi(s)$, by which the output deviation of the external control loop is given by $e_{DS} = r - \psi(s)y - [1 - \psi(s)]\, y_{ref}$. At lower frequencies $\omega \ll \omega_\psi$ while $|1 - \psi(j\omega)| \approx 0$ and $|P_K(j\omega)| \approx |P_n(j\omega)|$ as shown in (13), only the measured plant output y is connected to the feedback control loop, i.e. $e_{DS} \approx r - y$. The command tracking in (21) and sensitivity function in (22) are rewritten as

$$\hat{T}_{DS} \approx \hat{T}_{CK} = \frac{P_n C}{1 + P_n C}, \tag{24}$$

$$\hat{S}_{DS} \approx \hat{S}_{CK} = \frac{1}{(1 + P_n C)\,(1 + P_n K)}, \tag{25}$$

where the disturbance attenuation behaves like the double-loop control structure.

The control system will be switched to the reference feedforward control structure at higher frequencies $\omega \gg \omega_\psi$, where y_{ref} is adopted for the feedback control due to $|\psi(j\omega)| \approx 0$, i.e. $e_{DS} = r - y_{ref}$. The robust stability function in (23) is then simplified as

$$\Omega_{DS} \approx \Omega_K = \frac{P_n K}{1 + P_n K}, \tag{26}$$

which indicates the same allowable largest uncertainty margin as the reference feedforward control structure. Moreover, the feedback output is a mixed combination of y and y_{ref} around the breakpoint frequency of $\psi(s)$ such that the control system in Fig. 7(b) becomes a mixed TDOF control structure. In programming, the dynamic switching ψ is rewritten as $\psi(s) = \frac{\omega_\psi / s}{1 + \omega_\psi / s}$ and realized by $\frac{\omega_\psi}{s}$ with a negative unit feedback.

Remark 1: Instead of hard-switching, i.e. an equivalent case of $\psi = 1$ or $\psi = 0$, a new mixed TDOF control structure with a dynamic switching approach $\psi(s)$ is proposed .The control system can be provided with the double-loop control structure of Fig. 5 at lower frequencies $\omega \ll \omega_\psi$ while $|1 - \psi(j\omega)| \approx 0$ and the reference feedforward control structure of Fig. 6 at higher frequencies $\omega \gg \omega_\psi$ while $|\psi(j\omega)| \approx 0$.

Remark 2: In the proposed dynamic switching control, the controllers K and C can be independently designed for specific robust performances. Moreover, the frequency-dependent switching ψ endows the TDOF control structure to achieve the required multi-objective robustness requirements. The design procedures are briefly summarized by

i The internal compensator K should be designed for the robust stability such that $\left|\frac{1+P_nK}{P_nK}(j\omega)\right| \geq |W_u(j\omega)|$.
ii The desired robust tracking performance and disturbance attenuation are obtained by the external controller C.
iii A dynamic switching function of ψ with the bandwidth ω_ψ should satisfy $\omega_\psi < \omega_R$ such that $\left|1 + P_n C(j\omega_\psi)\right| > 1$.

V. SIMULATION AND EXPERIMENTAL VERIFICATIONS

In this study, a belt-driven servomechanism is utilized to realize the proposed switching control approach and verify

TABLE 1. Hardware specification of electric motor.

Quantity	Value
rated speed (RPM)	3000
rated torque (Nm)	6.37
maximum operating speed (RPM)	5000
maximum torque (Nm)	20.11
moment of inertia (kg·m^2)	0.0053
damping coefficient (Nm·s/rad)	0.0012

its feasibility and effectiveness. The hardware specifications of utilized motors are listed in Table 1.

A. DESIGN OF PROPOSED TDOF CONTROL FRAMEWORK

The preliminary derivation of a nominal model and its uncertainty bound of the belt-driven servomechanism are required for the following robust controller design. From the measured frequency responses (magnitude plot) as depicted in Fig. 2, a nominal model P_n is derived as

$$P_n(s) = \frac{K_t}{J\,s + B} = \frac{0.53}{0.0046s + 0.0012},$$

where J and B are the moment of inertia and damping coefficient, respectively. K_t is the torque constant of the motor. Note that the chosen low-order P_n can result in a lower order controller C design for robust tracking performance. The multiplicative uncertainty bound W_u defined in (1) is also found by

$$W_u(s) = \frac{2 \times 10^6 s}{\left(s + 3.1 \times 10^5\right)(s + 776.9)}$$

such that a frequency-dependent weight W_e is given by

$$W_e(s) = \frac{3823.7\,(s + 200)}{\left(s + 3.1 \times 10^5\right)(s + 776.9)}.$$

By the proposed method of weighting function selections, the constants $\alpha_e = 100\pi$ rad/ sec and $\alpha_u = 6.18$ Nm can be directly obtained from rated speed and torque specifications in Table 1. Accordingly, the shaped controlled plant P_s of (5) is determined by

$$P_s(s) = \alpha_e^{-1}\,\alpha_u\,W_e P_n\,W_{\mathrm{u}}^{-1} = \frac{2.55\,(s + 200)}{s\,(s + 0.26)}.$$

It can be seen that the selection of specific W_u and W_e, which are the coprime factorization, can prevent the order increment of P_s.

To synthesize the robust controller, let $\left[\begin{array}{c|c} A_s & B_s \\ \hline C_s & 0 \end{array}\right]$ denote the state-space realization of a transfer function $P_s(s) = C_s\,(sI - A_s)^{-1}\,B_s$, and let $P_s(s) = \tilde{M}_s^{-1}\tilde{N}_s(s)$ be the left coprime factorization. From [25], the normalized coprime factors $\tilde{N}_s$ and $\tilde{M}_s$ are derived as follows:

$$\left[\tilde{N}_s(s) : \tilde{M}_s(s)\right] \overset{s}{=} \left[\begin{array}{c|c:c} A_s + H\,C_s & B_s & H \\ \hline C_s & 0 & I \end{array}\right]$$

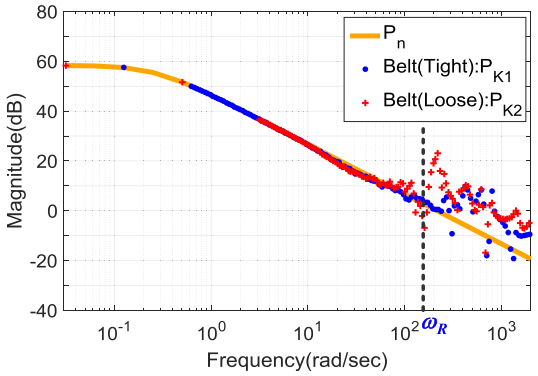

FIGURE 8. Robust internal-loop compensation.

$$= \left[\begin{array}{cc|c} -2.77 & -502.34 & 1 & -0.99 \\ 0.85 & -29.27 & 0 & -0.06 \\ \hline 2.55 & 509.95 & 0 & 1 \end{array}\right].$$

Moreover, the input weight W_d is given by

$$W_d(s) = \tilde{M}(s) \overset{s}{=} \left[\begin{array}{c|c} A_s + HC_s & H \\ \hline C_s & 1 \end{array}\right] = \frac{s\,(s + 0.26)}{s^2 + 32.04\,s + 509.9}$$

such that the poles of W_d are the same as that of P_s, and the zeros of W_d are the same with eigenvalues of $A_s + H\,C_s$. By the H_∞ control design theory [22] [25], the robust feedback controller K_∞, which satisfies (7) with $\gamma_o = 2.44$, can be found by

$$K_\infty(s) = \frac{1.12\,(s + 9.67)\,(s + 2688)}{(s + 48)\,(s + 1347)}.$$

By (8), the internal controller K is given as

$$K(s) = \frac{0.01\,(s + 9.67)\,(s + 200)\,(s + 2688)}{s\,(s + 48)\,(s + 1347)}.$$

The robustness of P_K based on the designed K is verified with different belt tensions as shown in Fig. 8, where P_{KT} and P_{KL} denote the internal control loop with P_T (tight) and P_L (loose), respectively. Based on the magnitude plot of Fig. 8, the upper frequency $\omega_R \approx 155.8$ rad/sec is obtained such that $P_K = \frac{P(1+KP_n)}{1+PK} \approx P_n$ is ensured within this frequency region. A classical design method can then be employed to find C for desired tracking performance.

The pole placement method is adopted here for the design of C. Let the external-loop controller be a proportional-integral (PI) controller, i.e., $C(s) = C_P + \frac{C_I}{s}$. Then, the command tracking in (14) can be given by

$$\hat{T}_{CK} = \frac{P_n C}{1 + P_n C} = \frac{K_t\,(C_P\,s + C_I)}{J\,s^2 + (B + K_t C_P)\,s + K_t C_I}.$$

Considering the desired natural frequency $\omega_C = 10$ Hz and damping ratio $\xi_C = 0.86$ for the output response without overshoot, the parameters of $C(s)$ are obtained by

$$C_P = \frac{2\xi_C\,\omega_C J - B}{K_t} \approx 0.45, \quad C_I = \frac{J\,\omega_C^2}{K_t} \approx 18.25.$$

The corresponding responses of $\hat{T}_{CK}$ and S_C are depicted in Fig. 9. Within the low frequency $\omega_R \approx 24.8$ Hz, $\hat{T}_{CK}$ can

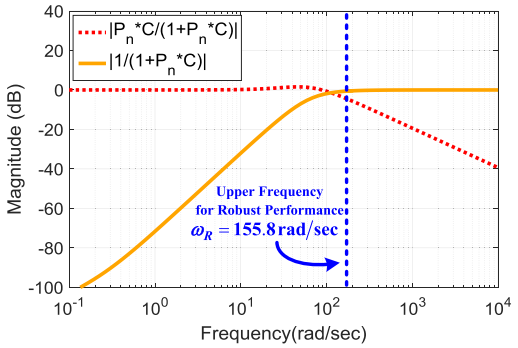

FIGURE 9. Design of external control loop.

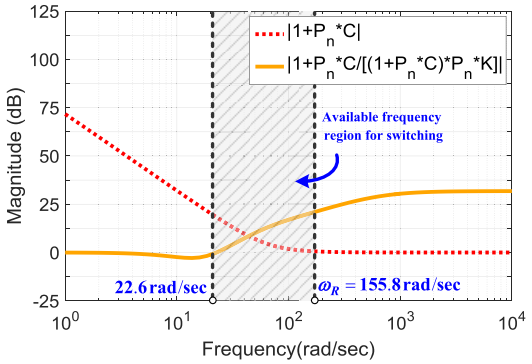

FIGURE 10. Design of proposed dynamic switching.

achieve the desired command tracking, and $|S_C(j\omega)| \leq 1$ can improve the disturbance attenuation.

An appropriate switching frequency region can be found based on the designed K and C as shown in Fig 10. The upper bound of the switching frequency ω_ψ is determined for the disturbance rejection, which satisfies

$$|1 + P_n C(j\omega)| > 1 \quad if\ \omega < \omega_R,$$

as well as the lower bound is given by $\omega_R \approx 155.8$ rad/sec for robust performance requirement in (13) such that

$$\left|1 + \frac{P_n C}{(1 + P_n C)\, P_n K}(j\omega)\right| > 1 \quad if\ \omega \geq 461.8\,\text{rad/sec}.$$

Thus, the dynamic switching frequency is selected as $\omega_\psi = 32$ rad/sec to achieve satisfactory disturbance rejection and robust stability.

B. SIMULATION RESULTS

The proposed TDOF switching control framework can be evaluated with different performance measurements. For the case of $P = P_n$, the command tracking T of four different control structures is compared as shown in Fig. 11(a). Undoubtedly, the TDOF control structure inherently has better dynamic tracking performance than that of the SDOF method, where the bandwidth can be improved from 34.51 rad/sec to 142.04 rad/sec. The disturbance attenuation is also measured as shown in Fig. 11(b). By the feedback of

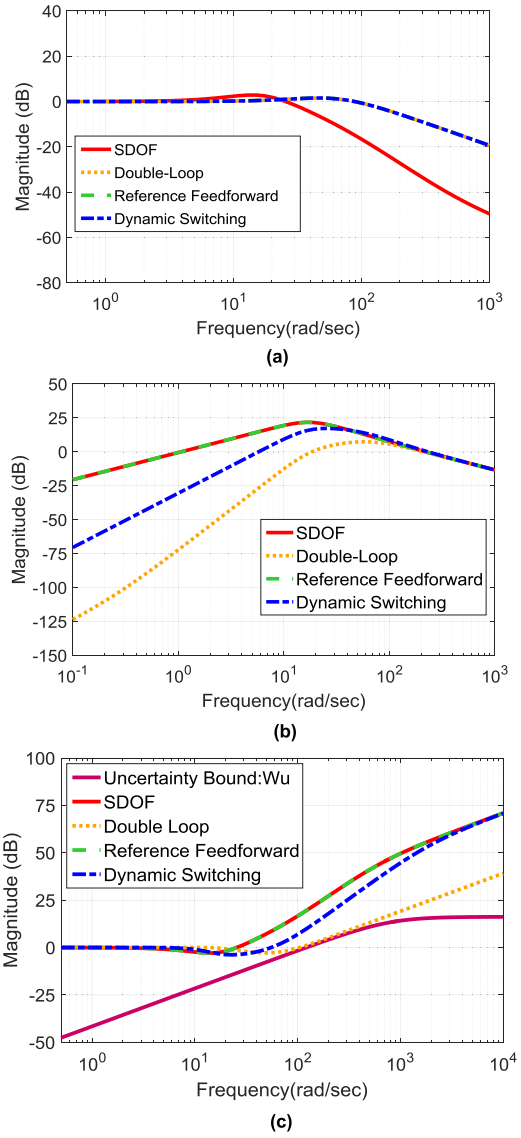

FIGURE 11. Performance measurements of different control frameworks. (a) Tracking performance. (b) Disturbance rejection. (c) Robust stability.

y, the output deviation caused by the disturbance is compensated not only by internal K but also external C. The double-loop control structure can improve the disturbance rejection at low-frequencies. However, it makes the control system close to the stability margin as depicted in Fig. 11(c). By contrast, the reference feedforward control structure has better robust stability at high frequencies, the same as that of the single DOF control structure in Fig. 3. The proposed dynamic switching approach shows the appealing merit of combining the control structures in Figs. 5 and 6. By dynamically switching output feedbacks of y and y_{ref}, as can be seen in Fig. 11, the control system can achieve both the desired disturbance rejection at low frequencies and robust stability for high-frequency uncertainties.

Considering the dynamic switching control structure in Fig. 7(b), its characteristic equation is given by

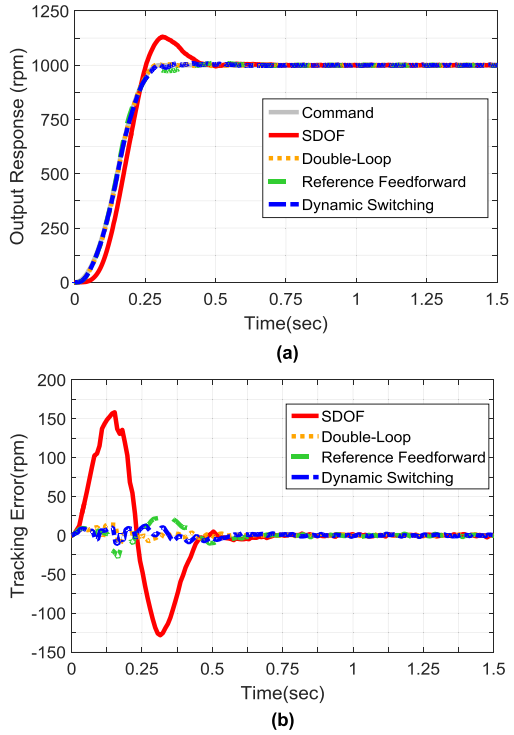

FIGURE 12. Tracking performance in different control frameworks. (a) Output response. (b) Tracking error.

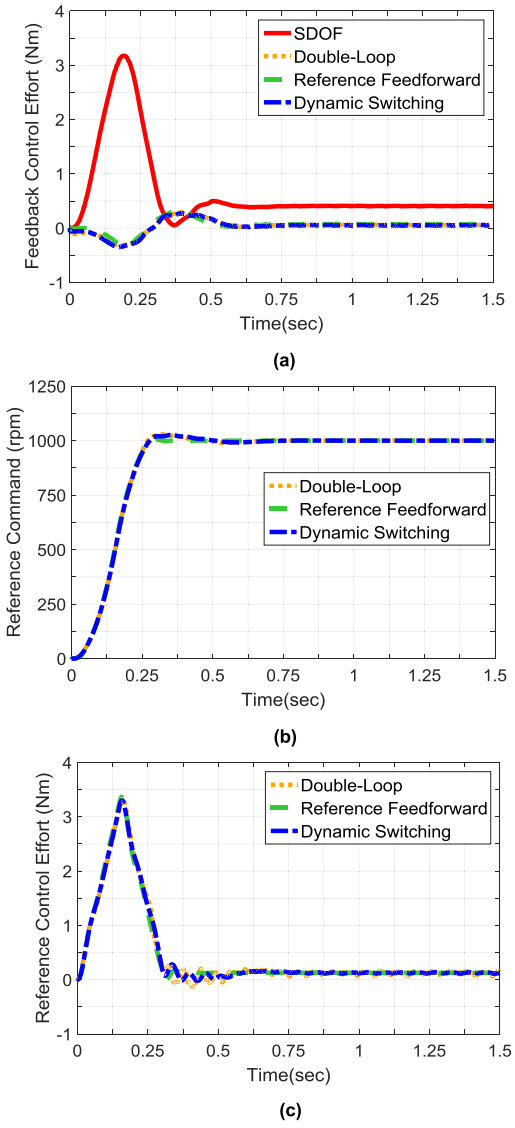

FIGURE 13. Control efforts in different control frameworks. (a) Feedback control efforts. (b) Feedforward Reference command. (c) Feedforward reference control effort.

$1 + \Delta W_u \Omega_K = 0$, where Ω_K is defined in (9), for the case of $\psi = 0$, and $1 + \Delta W_u \Omega_{CK} = 0$ for the case of $\psi = 1$, where Ω_{CK} is defined in (19). Note that the closed-loop control system is robust stable if $\|W_u \Omega_K\|_\infty \leq 1$ for $\psi = 0$, and then $\|W_u \Omega_{CK}\|_\infty \leq 1$ for $\psi = 1$. Based on the well-designed K, it can be found by (10) that $\|W_u \Omega_K\|_\infty \leq 1$. The control system would be dynamically switched by $\psi(j\omega)$ around the breakpoint switching frequency ω_ψ ($< \omega_R$). In the illustrated servomechanism design example, it can be verified that $\|W_u \Omega_K\|_\infty = 0.24$ and $\|W_u \Omega_{CK}\|_\infty = 0.89$. Therefore, the stability of the proposed dynamic switching control scheme shown in Fig. 7(b) can be guaranteed since $|\psi(\omega)| \leq 1, \ \forall \omega$.

C. EXPERIMENTAL RESULTS

The feasibility of the proposed dynamic switching TDOF control is also verified via the experimental results. In the used experimental setup of the belt-driven servomechanism, a velocity command $r = 1000$ rpm is applied for the motor speed control system. The measured velocity responses resulting from the SDOF and TDOF control approaches are depicted in Fig. 12. An s-curve function is applied to generate velocity command to avoid the saturation of the motor drive in practice. The control efforts, which involve the internal-loop feedback compensation, feedforward reference output y_{ref} and control input u_{ref}, are depicted in Fig. 13. As can be seen from Fig. 12(a), the TDOF control structures have better tracking performances than that of the SDOF approach, in which the tracking error is limited in the range of 0.2% as shown in Fig. 12(b).

A larger transient tracking error can be found in the SDOF control approach. The output deviation is only compensated by K as shown in Fig. 13(a). In the TDOF approaches, the reference command y_{ref} is generated by the external control loop to improve the transient response as depicted in Fig. 13(b). Moreover, the feedforward control effort u_{ref} will be the main control effort for command tracking such that the effects of uncertainty are eliminated by K as represented in Fig. 13(c).

Furthermore, an external torque disturbance $d = 1.6$ Nm is generated at $t = 5$ sec by the load-motor as shown in Fig. 14(a). The resultant tracking errors from 4 discussed control structures are represented in Fig. 14(b). Although the double-loop control structure has the best disturbance attenuation, the oscillation appearing in its output response

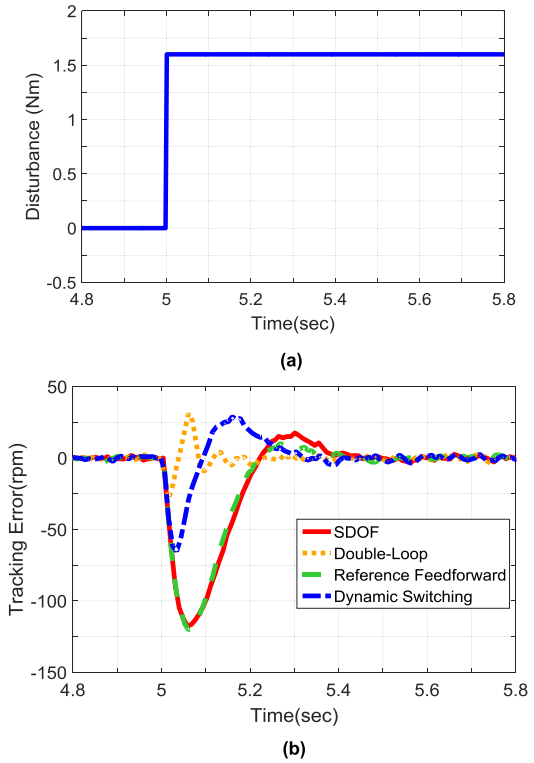

FIGURE 14. Performance measurements for disturbance attenuation. (a) External Disturbance. (b) Tracking error.

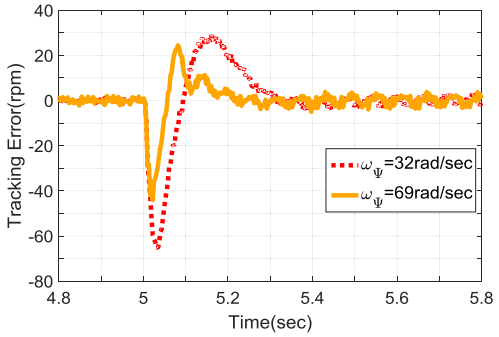

FIGURE 15. Performance with different switching frequencies.

indicates the lower relative stability of the control system. As SDOF control, the disturbance cannot be further rejected in the reference feedforward control structure because the external loop is merely a reference signal generator. To avoid the dilemma in control performances, the proposed dynamic switching control approach shows the flexibility to combine the two control structures. Without an obvious oscillation appearing in the output response, the proposed approach reveals that it can improve the disturbance rejection and also ensure better system stability through one fixed TDOF control structure.

Additionally, Fig. 15 shows the disturbance attenuations obtained from different chosen cut-off frequencies of ψ. It reveals that a higher cut-frequency leads to a better disturbance rejection with degradation in robust stability, where an obvious oscillation exists in the output response.

VI. CONCLUSION

This paper proposed a new TDOF control structure, which is capable of dynamically switching between the double-loop and reference feedforward control structures to achieve the different required control robustness. Based on the systematical and structural analysis, the proposed frequency-dependent switching control structure can enhance the disturbance rejection at lower frequencies. At higher frequencies, it also keeps the robust stability and improves the dynamic tracking based on the command feedforward. Without increasing the complexity, the design dilemmas appearing in conventional TDOF control approach can be resolved. A straightforward design procedure for the dynamic switching control approach is illustrated in ***Remark 2*** of Section III. A belt-driven servomechanism was further utilized to verify the feasibility and effectiveness of the proposed dynamic switching control approach.

ACKNOWLEDGMENT

This work was supported by the Ministry of Science and Technology (MOST), Taiwan, under Grant MOST 106-2221-E-006-251-MY3 and Grant MOST 106-2218-E-006-023.

REFERENCES

[1] A. Hace, K. Jezernik, and M. Terbuc, "Robust motion control algorithm for belt-driven servomechanism," in *Proc. IEEE Int. Symp. Ind. Electron.*, Jul. 1999, pp. 893–898.
[2] M. Araki and H. Taguchi, "Two-degree-of-freedom PID controllers," *Int. J. Control, Autom., Syst.*, vol. 1, no. 4, pp. 401–411, 2003.
[3] S. Srivastava and V. S. Pandit, "A 2-Dof LQR based PID controller for integrating processes considering robustness/performance tradeoff," *ISA Trans.*, vol. 71, pp. 426–439, Nov. 2017.
[4] H. Du, D. Cao, and H. Zhang, *Modeling, Dynamics, and Control of Electrified Vehicles*. Cambridge, U.K.: Woodhead, 2017.
[5] S. Morimoto and Y. Takeda, "Two-degrees-of-freedom speed control of resonant mechanical system based on H^{∞} control theory," *Elect. Eng. Jpn.*, vol. 117, no. 1, pp. 112–121, 1996.
[6] M. Kumar and V. V. Patel, "Tuning of two degree of freedom PID controller for second order processes," *Int. J. Sci., Eng. Technol. Res.*, vol. 4, no. 5, pp. 1543–1546, 2015.
[7] G. A. Hassaan, "Tuning of a feedforward 2DOF PID controller to control second order-like processes," *Int. J. Eng. Techn.*, vol. 4, no. 4, pp. 135–142, 2018.
[8] L. Kevickzy and C. Banyasz, *Two-Degree-of-Freedom Control Systems: The Youla Parameterization Approach*. New York, NY, USA: Academic, 2015.
[9] J. Singh, K. Chattterjee, and C. B. Vishwakarma, "Two degree of freedom internal model control-PID design for LFC of power systems via logarithmic approximations," *ISA Trans.*, vol. 72, pp. 185–196, Jan. 2018.
[10] T. Umeno and Y. Hori, "Robust speed control of DC servomotors using modern two degrees-of-freedom controller design," *IEEE Trans. Ind. Electron.*, vol. 38, no. 5, pp. 363–368, Oct. 1991.
[11] K. Nam, H. Fujimoto, and Y. Hori, "Motion control of electric vehicles based on robust lateral tire force control using lateral tire force sensors," in *Proc. IEEE/ASME Int. Conf. Adv. Intell. Mechatronics (AIM)*, Jul. 2012, pp. 526–531.
[12] B. K. Kim, H. T. Choi, W. K. Chung, and I. H. Suh, "Analysis and design of robust motion controllers in the unified framework," *J. Dyn. Syst., Meas., Control*, vol. 124, no. 2, pp. 313–321, 2002.
[13] B. K. Kim and W. K. Chung, "Unified analysis and design of robust disturbance attenuation algorithms using inherent structural equivalence," in *Proc. Amer. Control Conf.*, 2001, pp. 4046–4051.

[14] M.-C. Tsai, F.-Y. Yang, and C.-L. Chun, "A double-loop control structure for tracking control and disturbance attenuation," *IFAC Proc.*, vol. 47, no. 3, pp. 204–209, 2014.
[15] K. Ohishi, M. Nakao, K. Ohnishi, and K. Miyachi, "Microprocessor-controlled DC motor for load-insensitive position servo system," *IEEE Trans. Ind. Electron.*, vol. IE-34, no. 1, pp. 44–49, Feb. 1987.
[16] J.-S. Hu, D. Yin, and Y. Hori, "Fault-tolerant traction control of electric vehicles," *Control Eng. Pract.*, vol. 19, no. 2, pp. 204–213, 2011.
[17] B.-K. Choi, C.-H. Choi, and H. Lim, "Model-based disturbance attenuation for CNC machining centers in cutting process," *IEEE/ASME Trans. Mechatronics*, vol. 4, no. 2, pp. 157–168, Jun. 1999.
[18] H.-T. Choi, B. K. Kim, and K.-S. Eom, "A new framework for two loop disturbance rejection control," *Int. J. Control*, vol. 79, no. 6, pp. 636–649, 2006.
[19] Y. Ebihara, Y. Fujiwara, T. Hagiwara, and M. Sato, "2DOF control system design for maneuverability matching and gust disturbance rejection in in-flight simulator MuPAL-α," in *Proc. SICE Annu. Conf.*, 2010, pp. 524–528.
[20] G. Roppenecker, "State feedback control of linear systems—A renewed approach," *Automatisierungstechnik*, vol. 57, no. 10, pp. 491–498, 2009.
[21] M. Zeitz, "Vorsteuerungs-Entwurf im Frequenzbereich: Offline oder Online," *Automatisierungstechnik*, vol. 60, vol. 60, pp. 375–383, 2012.
[22] M.-C. Tsai, and D.-W. Gu, *Robust and Optimal Control: A Two-port Framework Approach*. London, U.K.: Springer-Verlag, 2014.
[23] K. Glover and D. McFarlane, "Robust stabilization of normalized coprime factor plant descriptions with H_∞-bounded uncertainty," *IEEE Trans. Autom. Control*, vol. 34, no. 8, pp. 821–830, Aug. 1989.
[24] J. Whidborne, I. Postlethwaite, and D.-W. Gu, "Robust controller design using H_∞ loop-shaping and the method of inequalities," in *Proc. IEEE Conf. Decis. Control*, Dec. 1993, pp. 2163–2168.
[25] B.-H. Shen and M.-C. Tsai, "Robust dynamic stiffness design of linear servomotor drives," *IFAC J. Control Eng. Pract.*, vol. 14, pp. 1325–1336, Nov. 2006.

CHUN-LIN CHEN (S'10) was born in Hsinchu, Taiwan, in 1986. He received the B.Eng. degree in mechanical engineering from National Chung Cheng University, Taiwan, in 2009, and the M.Sc. degree in mechanical engineering from National Cheng Kung University, Tainan, Taiwan, in 2011, where he is currently pursuing the Ph.D. degree with the Department of Mechanical Engineering.

He is the author of one published journal papers, and he is a holder of one Taiwan patent. His current research interests include motion control, robust control, and transmission control.

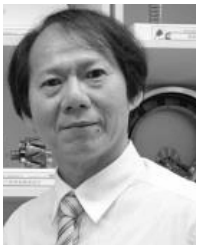

MI-CHING TSAI (S'87–M'89–SM'98) received the Ph.D. degree in engineering science from the University of Oxford, Oxford, U.K., in 1990.

He is currently a Chair Professor at the Department of Mechanical Engineering, National Cheng Kung University, Taiwan. He has authored or co-authored more than 117 journal papers and holds more than 117 patents. His research interests include robust control, servo control, motor design, and applications of advanced control technologies using DSPs.

Dr. Tsai is a fellow of the Institution of Engineering and Technology, U.K. He was an Associate Editor of the IEEE/ASME Transactions on Mechatronics from 2003 to 2007 and the Deputy Minister of Ministry of Science and Technology, Taiwan, from 2016 to 2017.